900–911 Nucleic Acids Research, 2013, Vol. 41, No. 2 Published online 27 November 2012
doi:10.1093/nar/gks1121

Eroded human telomeres are more prone to remain uncapped and to trigger a G2 checkpoint response

Laurent Jullien, Marie Mestre, Pierre Roux and Véronique Gire*

Universités Montpellier 2 et 1, CRBM-CNRS UMR 5237, 1919, route de Mende, 34293 Montpellier, France

Received July 25, 2012; Revised October 18, 2012; Accepted October 22, 2012

ABSTRACT

Telomeres cap the ends of chromosomes and regulate the replicative life span of human somatic cells. Telomere function is lost upon critical shortening and a p53-dependent checkpoint that detects altered telomere states at the G1/S transition was proposed to act as a regulator of the telomere damage response. We show that telomerase-negative human fibroblasts spend more time in G2 phase as they approach senescence and this delay is associated with manifestations of telomere dysfunction and the triggering of an ATM/ATR-dependent DNA damage signal. This correlates with a partial release of telomeric proteins TRF1 and TRF2. Analysis of the consequences of TRF1 and TRF2 depletion or over-expression of mutated versions revealed that telomere uncapping or telomere replication stress also led to DNA damage signalling in G2. Progression through mitosis of these cells was associated with signs of incomplete telomere terminal processing. We also observed an increase in sister chromatid-type telomere aberrations in senescing fibroblasts indicating that defects of telomere post-replicative events increased as cells age. Our results link a post-replicative damage response at eroded telomeres to G2 arrest signalling and challenge the current paradigm that the checkpoint response to short telomeres occurs primarily at the G1/S transition in human cells.

INTRODUCTION

Telomeres are dynamic nucleoprotein structures that play a critical role in maintaining chromosome stability and cell viability (1). Human telomeres consist of tandem TT AGGG repeats and end with a 3′ single-stranded G-rich overhang, which is thought to fold back into the duplex telomere DNA to create the T-loop structure (1,2). Key regulators of telomere structure and length include double-stranded (TRF1 and TRF2) and single-stranded (POT1) telomere DNA binding proteins and interconnectors (Rap1, TIN2 and TPP1), which all together form the shelterin complex (2). Although the shelterin complex shields chromosome ends from unwanted repair activities, it does not render the telomere invisible to the cell surveillance machinery. Rather, it creates a unique identity for the telomere, so that telomeres become transiently uncapped following their replication in S phase and the recruitment of DNA damage repair proteins ensures the correct reassembly of the telomere protective structures in G2 (3,4).

Telomere length is maintained by telomerase that offset loss of telomere sequences during DNA replication or nucleolytic processing (5). However, telomerase activity is absent in most human somatic cells and thus telomeres continuously shorten as cells divide, ultimately leading to loss of telomere function. Normal cells respond to short telomeres by activating the Ataxia Telangiectasia Mutated (ATM)-regulated DNA damage response and initiating replicative senescence (6–8). Telomerase expression, which halts telomere erosion, prevents senescence and allows cells to divide indefinitely (9) and consequently, the accumulation of too short telomeres is believed to trigger senescence. However, the precise events that occur at short telomeres remain unclear. Telomere length is probably not the sole factor determining the onset of senescence. Indeed, in most human senescent cells, telomeres are still quite long, often averaging 5–10 kb (5,10). Conversely, most of cancer cell lines carry much shorter telomeres yet retain the ability to divide (11,12). Moreover, TRF2 over-expression accelerates telomere shortening, resetting the shortest-tolerated telomere length to a lower value, but does not affect the onset of senescence (13). The delay of senescence is not solely due to inhibition of the senescence signalling pathway by excess TRF2, as telomeres in these cells are also protected from the fusions that would accompany equivalent levels of telomere shortening in cells with normal TRF2 levels. Since, short telomeres *per se* are not incompatible with continued cell division, a more complex structural determinant or a threshold level of shelterin proteins required to maintain telomere function may be involved (14).

*To whom correspondence should be addressed. Tel: +33 434359513; Fax: +33 434359410; Email: veronique.gire@crbm.cnrs.fr

We hypothesized that eroded telomeres are vulnerable to uncapping during or just after telomere replication. There is evidence that the shortest telomere(s) and not their average length trigger senescence in mouse (15) and that the G2/M cell cycle arrest of senescent yeast cells may be due to a replication problem of the shortest telomere (16). Replication of both the leading and lagging strands requires the temporarily disruption of the telomere 3D structure by the passage of the replication forks. Loss of telomere sequences due to end-replication problems occurs precisely during this phase of telomere replication at the lagging strand. In addition, telomere ends might be subjected to exonucleolytic attack, which may further exacerbate the instability of critically short telomeres (17). Unlike chromosome ends with sufficient reserve of telomere repeats and/or telomere binding proteins, a short telomere may not support the formation of a stable conformation after replication. The link between cell cycle progression and telomere uncapping is supported by studies in which shelterin components are inactivated or silenced. For instance, inhibition of TRF2 by a dominant negative allele in human cells or by targeted deletion in mice causes rapid uncapping of telomeres and fusion of chromosome ends via the non-homologous end joining (NHEJ) machinery in both G1 and G2 phases of the cell cycle (18–20). Targeted deletion of *Trf1* in mice revealed that telomere regions represent fragile sites and require TRF1 for their efficient replication (21,22). Upon *Trf1* deletion, stalled replication forks accumulate within the telomere repeats, activating a DNA damage response at telomeres that results in senescence in the absence of telomere shortening (21,22). Inactivation of shelterin proteins in p53-deficient mouse embryo fibroblasts and immortal cancer cell lines allows mitotic entry in the presence of uncapped telomeres (23). In such models of telomere dysfunction, some telomere uncapping could be expected on every telomere as opposed to what observed in normal human cells approaching senescence, where telomere uncapping occurs gradually due to the loss of telomeric sequences, resulting in the inability to bind to shelterin components. Little is known about the relationship between the assembly of the post-replicative telomere cap and the cell cycle surveillance machinery during physiological telomere shortening. We investigated here the primary response to telomere shortening in primary human fibroblasts by examining the timing of DNA damage response activation and cell cycle arrest as these cells were losing growth potential. We found that post-replicative eroded telomeres in senescing human fibroblasts recruit DNA damage response factors in G2 and that this telomere damage signalling is associated with p53-dependent delay in G2.

MATERIALS AND METHODS

Cell culture and treatments

WI-38 and IMR-90 fibroblasts were from the American Type Culture Collection. HFF fibroblasts have been described (8). Cells were cultured in Modified Eagle's Medium supplemented with 10% foetal calf serum (FCS), 1% non-essential amino acids, 1 mM sodium pyruvate, 2 mM glutamine and 100 U/ml penicillin/streptomycin (GIBCO BRL). Cells were pre-synchronized in G0 by contact inhibition and then released into the cell cycle by dilution. Cells were then arrested at the G1/S boundary by addition of 2 mM hydroxyurea and 12 h incubation, then washed and released in fresh media as described (24). Caffeine was added at 10 mM for 16 h where indicated.

SA-β-gal staining was carried out as described (8). The bromodeoxyuridine (BrdU) labelling index was determined by dual immunofluorescence following BrdU incorporation for 1 or 24 h, as described (8).

Retroviral infection and transfection

Retroviral plasmids used were as follows: TRF1, ΔATRF1, ΔMTRF1, ΔAΔMTRF1 (Flag-tagged), TRF2 and ΔBΔMTRF2 (Myc-tagged) in pLPC vector [described in (13,18,25) and gifts from Dr T. de Lange]. pLXSN-HPV-E6/E7 was a gift from D. Galloway. pRETROSuper-sh*GFP*, -sh*p53* and sh*ATM* were gifts from F. D'Adda di Fagagna. Methods used for retroviral production and infection have been described (8). Infections were performed sequentially and infected cell populations were selected with 400 μg/ml G418 for pLXSN plasmids and 1 μg/ml puromycin for pLPC and pRETROSuper constructs. Retroviral vectors carrying only drug resistance genes were used as controls.

For RNA interference experiments, cells were transfected with 20 nM of *siATM*, *siATR,* si*TRF1* and si*TRF2* SMARTpool and control si*GFP* (synthesized by Dharmacon) using Oligofectamine (Invitrogen), as described (8).

Cell fractionation

Cells were suspended in cytoplasmic extraction buffer (CEB) [10 mM HEPES, pH7.9, 10 mM KCl, 0.1 mM EDTA, 0.1 mM EGTA, 1 mM DTT, 1 mM PMSF, 0.1 mM sodium vanadate, and protease inhibitors cocktail (Sigma)] and incubated on ice for 10 min. Supernatants were collected as cytoplasmic fractions by centrifugation at 1300 *g* at 4°C for 5 min. Pellets were suspended in nuclear extraction buffer (NEB) (3 mM EDTA, 0.2 mM EGTA, 1 mM DTT, 1 mM PMSF, protease inhibitors) and incubated on ice for 30 min. Supernatants were collected as soluble nuclear fractions by centrifugation at 1700*g* at 4°C for 5 min. To release chromatin-bound proteins, pellets were suspended in NEB with 1 mM $CaCl_2$ and 0.3 U micrococcal nuclease (Sigma) and incubated at 37°C for 2 min. The insoluble pellet was removed from the chromatin-bound fraction by centrifugation at 13 000*g* at 4°C for 5 min.

Western-blot analysis

Cells were lysed and analysed by immunoblotting as described (8). Primary antibodies were as follows: anti-p53 (DO-1), -p21Waf1 (sc-347), -Chk1 (G4), -Cdk2 (sc-163), Cdk4 (sc-260), Cyclin E (HE-12) (Santa Cruz Biotechnology), -S15-p53, -T68-Chk2, -S345-Chk1-S317-Chk1, S1981-ATM (10H11.E12) (all from

Cell Signaling Technology), -Chk2 (clone 7, Millipore), -ATM, -ATR, hRap1 (Bethyl Laboratories), -p16INK4a (G175-405), -pRB (G3-245), -Cyclin D1 (G124-326, Bio sciences Pharmingen), Histone H3, γ-H2AX (JBW301, Upstate Biotechnology), -TRF2 (4A794, Imgenex), -TRF1 (57-6, Novus Biologicals and TRF-78, Abcam), -POT1 (Novus Biologicals), -TIN2 (gift of S-H Kim, Detroit, USA), -Cyclin A (6E6, Novocastra), -Flag (F-7425), -γ-Tubulin (GTU 88) and -α-Tubulin (DM1A) (Sigma). As secondary antibodies, HRP-linked anti-mouse or anti-rabbit (GE Healthcare) were used.

Immunoprecipitation and kinase assay

Cells were lysed and immunoprecipitation was carried out as described (24), using an anti-Cyclin A (sc-751, Santa Cruz) antibody. Kinase activities were determined by incubating beads with Histone H1 (2 μg, Roche) in kinase reaction buffer (20 mM Tris pH 7.5, 15 mM $MgCl_2$) with 250 mM ATP and 0.2 μl ^{32}P-γ-ATP (10 μCi/μl) at 30°C for 30 min. Samples were fractionated by SDS–PAGE and gels were stained with Coomassie blue, dried and the Histone H1 bands excised and quantified using a scintillation counter.

ChIP assay

Cells synchronized as above were fixed with 1% formaldehyde for 1 h and ChIP assay was performed as described (8). Polyclonal anti-TRF1 and anti-TRF2 antibody (for ChIP application, Santa Cruz) and control ChIP grade IgG (Abcam) were used. Real time PCR analysis was performed using the primer sets specific for telomere (26). PCR amplification conditions were as follows: 10 min at 95°C, followed by 40 cycles of 30 s at 95°C and 2 min at 54°C. Reactions were normalized to the control antibody and fold changes in the levels of association above background was calculated using the following equation $[1/(2A)] \times 100$. The values were then adjusted to the values of input samples.

Immunofluorescence and telomere fluorescence *in situ* hybridization (PNA-FISH)

Cells grown on coverslips were analysed by immunofluorescence as described (8) with the primary antibodies described in the western-blot section. After overnight incubation at 4°C, antibody binding was revealed with goat secondary antibodies conjugated to Texas-red or Alexa Fluor (Alexa 350 and 488) (Molecular Probes). Then, cells were fixed in methanol:acetic acid (3:1, v:v) for 20 min and air dried. Metaphase spreads were prepared from cultures incubated with 0.1 μg/ml colcemid (Irvine Scientific, Santa Ana, USA) for 3–4 h, trypsinized, swollen in hypotonic buffer (20% FCS in H_2O) at 37°C for 10 min and fixed with methanol:glacial acidic acid (3:1, v:v). Cells were incubated with 0.5 μg/ml of a FITC-OO-$(CCCTAA)_3$ PNA telomere probe (Dako) in hybridization solution (70% formamide, 0.5% blocking reagent, 10 mM Tris–HCl at pH 7.2), denaturated at 82°C for 20 min and hybridized overnight at room temperature. Cells were then washed with PBS-0.1% Tween-20 at 57°C for 20 min and rinsed in 2×SSC-0.1% Tween-20 at room temperature for 1 min. Chromosomes were counterstained with 0.1 μg/ml Hoechst.

Terminal restriction fragment (TRF) length analysis

Genomic DNA was extracted using the DNeasy Tissue kit (Qiagen). A total of 3 μg were digested with HinfI and RsaI and resolved by 0.7% Tris–acetate–EDTA agarose gel electrophoresis. Telomere fragments were detected by Southern blotting with a single-stranded $(CCCTAA)_3$ telomeric probe and autoradiography. Autoradiographs were scanned with a densitometer and the mean telomere length was determined by quantifying the smear of hybridized fragments with the Molecular Analyst software (Bio-Rad) and an Excel spreadsheet designed to calculate the mean telomere length using the formula described in (5).

Image acquisition and image deconvolution

Images were captured with a DMRA Leica epifluorescence microscope, a plan apochromat ×100 oil objective (numerical aperture 1.4) and a 12 bits CoolSnap HQ2-cooled charge-coupled device camera (Photometrics, Tucson AZ) driven by the Metamorph 7.1 software (Universal Imaging Corporation). Nuclear size was quantified from digital images using the Metamorph advanced measure module.

Images were collected at 500 nm *z*-intervals from a series of 10 focal planes for the red and green channels. Images were processed using the classic maximum likelihood estimation algorithm of the Huygens professional software (Scientific Volume Imaging BV, Hilversrum, The Netherlands). Deconvolved images were imported into the Imaris program (Bitplane AG, Zurich, Switzerland) where PNA focal volumes were determined by generating 3D reconstructions under Surpass. The section with the largest volume area (presumed middle of the dot) was used for quantitative analysis. Images were pseudo-coloured with Metamorph 7.1.

Statistical analyses

The statistical significance between means was assessed with the unpaired Student's two-tailed *t*-test, with $P < 0.01$ considered as statistically significant.

RESULTS

Short telomeres trigger a DNA damage response during G2 phase

Foci of phosphorylated H2AX (γ-H2AX) are markers of the ATM and ataxia telangiectasia and Rad3-related (ATR)-regulated DNA damage responses, but they are also associated with dysfunctional telomeres, including short (6–8), unprotected (28) and damaged (21,22) telomeres. To investigate the timing of γ-H2AX recruitment to telomeres during replicative aging of human primary foreskin fibroblasts (HFF), we determined BrdU incorporation, telomere length and γ-H2AX telomere dysfunction-induced foci (TIFs) formation in individual cells using immunofluorescence and telomere PNA-FISH. γ-H2AX

began to be recruited to telomeres very early, when telomeres started to shorten and accumulated as far as 10–20 population doublings (PDs) away from full senescence at PD87 (Figure 1A). The PNA-FISH data correlated well with the results obtained using terminal restriction fragment (TRF) length analysis, an independent technique that does not rely on fluorescence, but on Southern-blot analysis of restriction enzyme-digested genomic DNA (see 'Materials and Methods' section) ($P = 0.0001$) (Supplementary Figure S1).

Quantification of the number of TIF-positive cells throughout the cell cycle indicated that, pre-senescent (PD70) fibroblasts were enriched in TIFs in the G1 and G2 phases, but rarely in mitotic cells (Figure 1B). The telomeric damage signal observed in G1 pre-senescent cells highlighted a subpopulation of cells that are undergoing early senescence. Indeed, the BrdU labelling index in pre-senescent cultures decreased to 35%, and 25% of the cells displayed β-galactosidase activity at pH 6 (SA-βGal; a biomarker of senescence) [Figure 1A and data not shown; see also (8)]. To make sure that tetraploid pre-senescent cells in the G1 phase of the cell cycle were not included in the G2 population based on their DNA content, we evaluated also the expression of Cyclin A, a S/G2 marker. Most of the cells that displayed high levels of Cyclin A contained also many TIFs (Figure 1C and D), arguing against the possibility that G1-arrested tetraploid cells were included in the G2 group.

TIFs accumulation in G2 in pre-senescent cells might be the result of damage due transient uncapping of telomeres following replication (3) in line with the immunofluorescence data in young cells (Figure 1B) or it could be due to short telomeres that persist uncapped during or after replication. Therefore, we assessed whether γ-H2AX accumulation was related to telomere length in pre-senescent fibroblasts using telomere PNA-FISH and dual immunofluorescence to detect γ-H2AX and Cyclin A in the same preparation. On the basis of the PNA-FISH signal intensity, we found that among the Cyclin A-positive cells, those with shorter telomeres showed a higher incidence of telomeric γ-H2AX staining (Figure 2A and B), as indicated also by the significant negative correlation ($P < 0.0001$) between telomeric γ-H2AX staining and telomere fluorescence intensity (Figure 2C). We therefore conclude that the incidence of telomeric γ-H2AX staining in G2 phase of pre-senescent cells relative to young cells arise from short telomeres that might have remained dysfunctional during or after their replication and were more prone to remain uncapped.

Next, we tested whether the increased telomeric damage observed in pre-senescent fibroblasts during G2 could lead to activation of the DNA damage machinery. Cells at

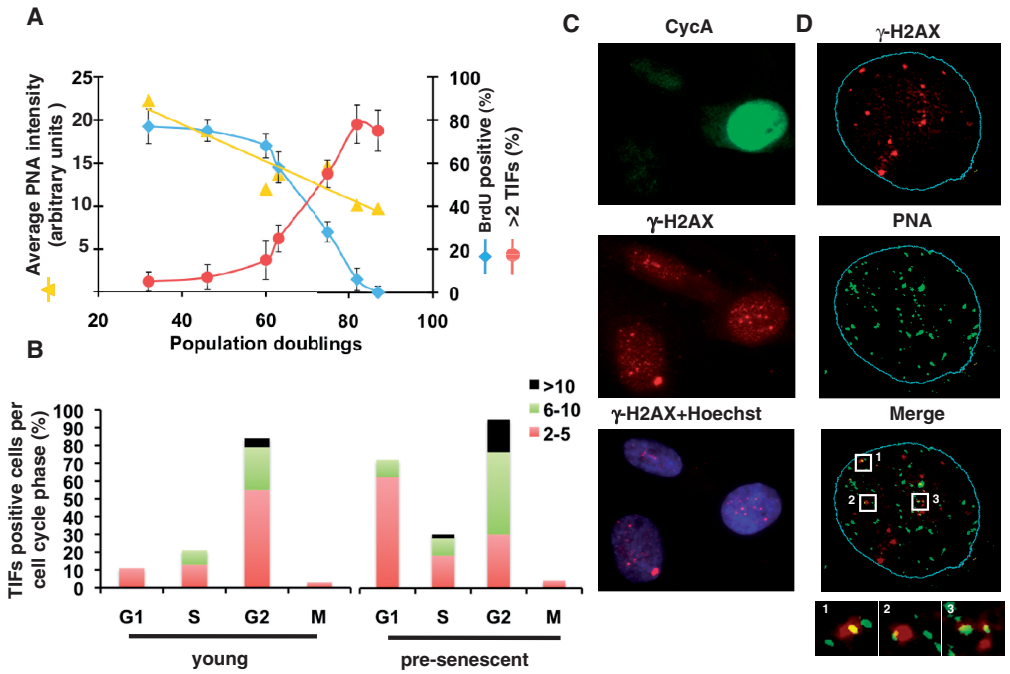

Figure 1. Accumulation of γ-H2AX foci at telomeres during late S/G2 in pre-senescent fibroblasts. (**A**) Telomere length, proliferative index and γ-H2AX foci formation were monitored in HFF cells cultured until replicative senescence (PD87). Cells at the indicated PDs were analysed for DNA synthesis (BrdU incorporation >24 h) or processed by telomere PNA-FISH to visualize γ-H2AX foci and telomeres. Plotted are the percentage of cells with at least two colocalized γ-H2AX/PNA foci (TIFs), the percentage of BrdU-positive cells and the mean value of the relative fluorescence intensity of individual telomere signals measured in 20 nuclei by quantitative FISH (see 'Materials and Methods' section). (**B**) Quantification of TIF frequency at each phase of the cell cycle. Young (PD32) and pre-senescent (PD70) cells were prepared as in (A) and stained with Hoechst. DNA measurement of Hoechst-stained cells by fluorescence microscopy was used to identify cells in G1, S and G2 phases. At least 100 cells from two independent experiments were analysed. Different colours indicate the number of TIFs/cell. (**C**) Immunofluorescence detection of γ-H2AX foci in HFF cells at PD70. Cells were stained with anti-Cyclin A (green) and anti-γ-H2AX (red) antibodies. Nuclei are blue in the combined γ-H2AX and Hoechst image. (**D**) Immunofluorescence detection of γ-H2AX foci (red) combined with telomere PNA-FISH (green) of a Cyclin A-positive fibroblast at PD70. Images are a single focal plane from a deconvolved 3D image. The white rectangles indicate TIFs and images on the bottom show boxed images at higher magnification. Nuclei are outlined in blue.

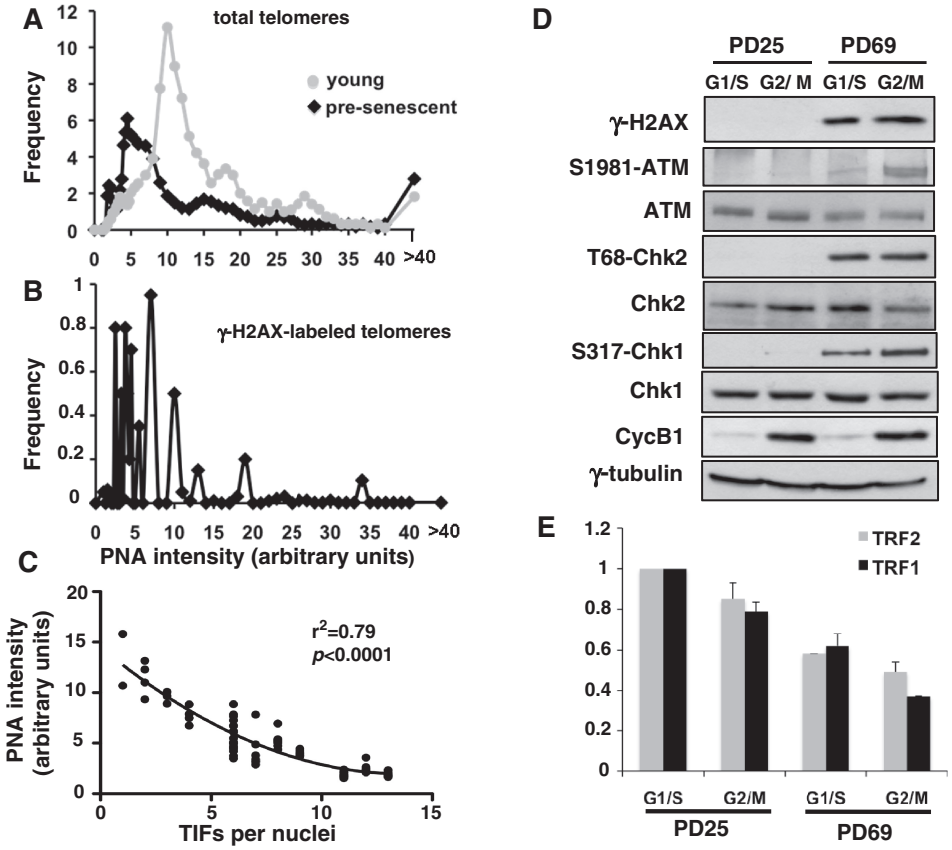

Figure 2. Activation of the DNA damage response during G2 correlates with short telomeres and reduced TRF1 and TRF2 binding in pre-senescent fibroblasts. (**A**) Data from Figure 1A reformatted to plot the distribution of telomere FISH signals in young (PD32) and pre-senescent cells (PD75). Fluorescence intensity was counted into intervals and plotted as the percentage of the total telomeres analysed. (**B**) γ-H2AX associates with eroded telomeres. The fluorescence intensity of individual telomeric FISH signals in pre-senescent cells (PD75) was examined by fluorescence microscopy and their association or not with γ-H2AX was recorded. The analysis includes 3165 telomeres, of which 196 stained positive for γ-H2AX. Results are expressed as in (A). (**C**) Second order polynomial regression analysis was used to assess the correlation between telomere fluorescence intensity and TIFs number in pre-senescent fibroblasts (data from Figure 2B). (**D**) Expression of DNA damage markers in cell extracts from synchronized young (PD25) and pre-senescent (PD69) HFF cells. Cells were synchronized at the G1/S transition via hydroxyurea block and released to re-enter the cell cycle. Blots were probed for γ-H2AX, ATM phosphorylation on serine 1981 (S1981-ATM), ATM, Chk2 phosphorylation on threonine 68 (T68-Chk2), Chk2, Chk1 phosphorylation on serine 317 (S317-Chk1) and Chk1 expression. Expression of Cyclin B1, a marker for the G2/M transition, was used to monitor cell cycle progression after release from the G1/S block. γ-Tubulin served as loading control. (**E**) Recruitment of TRF1 and TRF2 to telomeres monitored by quantitative ChIP assays using real-time PCR. Cells were prepared as in (D). Average fold changes in the association of TRF1 and TRF2 at telomeres from at least three experiments are plotted and error bars represent SD.

PD69 showed activation of key molecules involved in the DNA damage response, such as phosphorylation of ATM on Ser 1981 and its target checkpoint kinases Chk2 (on Thr 68) and Chk1 (on Ser 317) in G2/M phase (Figure 2D). Conversely, phosphorylated Chk2 and Chk1 kinases were not detected in young cells (PD25) in G2/M (Figure 2D), consistent with the notion that in young cells the DNA damage response is activated only locally at telomeres in G2 to promote the reassembly of a protective structure in newly replicated telomeres (3,4).

Persistence of TIFs in G2 is associated with reduced TRF1 and TRF2 binding

To assess whether γ-H2AX accumulation was linked to changes in telomere chromatin, we performed quantitative real-time PCR for telomere repeats following chromatin immunoprecipitation (ChIP) of cross-linked chromatin of young and pre-senescent HFF cells (26). We compared TRF1 and TRF2 occupancy of telomeres and found reduced binding of both proteins in pre-senescent HFF cells (Figure 2E). Western blotting confirmed that comparable levels of immunoprecipitated TRF1 and TRF2 were retrieved following the ChIP assay among the different conditions (Supplementary Figure S2B).

Next, we inhibited TRF1 and TRF2 function at telomeres to evaluate whether the persistence of TIFs in G2 was indicative of telomere protection dysfunction. Similar results were obtained either by generating stable cell lines with constructs that encode dominant negative TRF1 and TRF2 mutants, which lack the Myb DNA binding domain (ΔMTRF1 and ΔBΔMTRF2) (13,25) or by transfection of siRNAs against TRF1 and TRF2. The number of cells containing γ-H2AX foci increased significantly in cells with impaired TRF1 and TRF2 function relative to control cells (Figure 3A). Up to 60% of the γ-H2AX signal co-localized with telomeres as indicated by telomere PNA-FISH, in cells in which TRF1 (ΔMTRF1 or siTRF1) or TRF2 (ΔBΔMTRF2 or siTRF2) activity

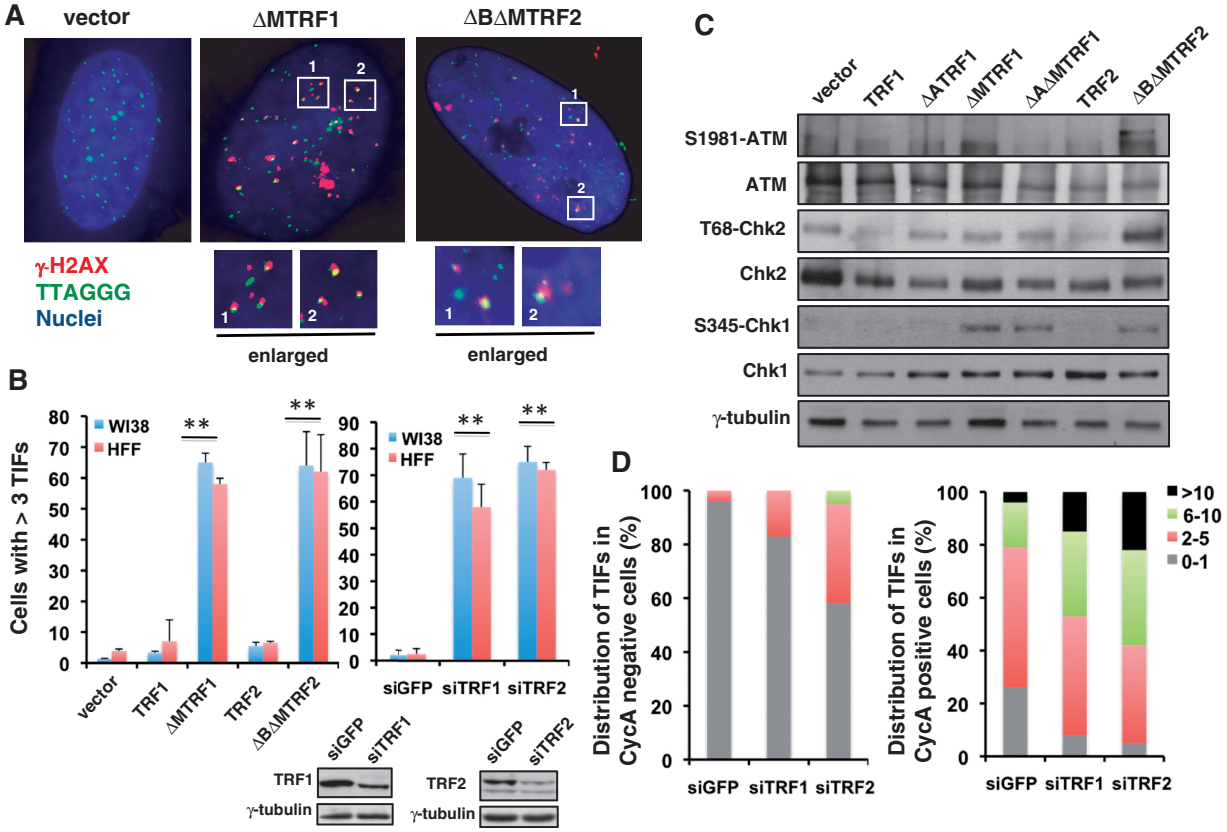

Figure 3. TIF induction during late S/G2 and DNA damage response activation upon telomere uncapping. (**A**) Images of telomeric γ-H2AX detection in WI-38 cells expressing the indicated retroviral constructs. Cells were analysed at day 8 after infection. Expression of Flag-ΔMTRF1 and Myc-ΔBΔMTRF2, using anti-Flag or anti-Myc antibodies (blue), was assessed concomitantly with that of γ-H2AX (red). Telomeres (TTAGGG, green) were detected by PNA-FISH. Hoechst staining of DNA in control cells (vector alone) is shown. The white rectangles indicate TIFs and images on the bottom show boxed image at higher magnification. (**B**) Quantification of γ-H2AX and telomeres colocalization in WI-38 and HFF cells expressing the indicated plasmids (left panel) or siRNAs (right panel). Shown is the percentage of cells with more than three foci in which γ-H2AX co-localized with telomere (TIFs). Statistical significance compared with controls (vector alone or siGFP) was assessed with the Student's *t*-test (**$P < 0.001$). Western blot of TRF1 and TRF2 expression in si*GFP* (control), si*TRF1* or si*TRF2*-transfected HFF is shown (lower panel). (**C**) Immunoblot analysis of ATM, Chk2 and Chk1 phosphorylation in WI-E6/E7 cells expressing the indicated retroviral plasmids. Cells were analysed at day 8 after infection. Blots were probed for S1981-ATM, ATM, T68-Chk2, Chk2, S345-Chk1 and Chk1 expression. γ-Tubulin served as loading control. ΔATRF1 is a mutant of TRF1 that lacks the TRF1 acidic domain. ΔAΔMTRF1 is a dominant-negative mutant of TRF1 that lacks both the Myb DNA binding and acidic domains. (**D**) Quantification of TIF-positive cells following transfection with si*TRF1*, si*TRF2* or si*GFP*. Cells were immunolabeled with anti-γ-H2AX and anti-CyclinA antibodies 48 h after transfection. Cyclin A is expressed throughout the S and G2 phases of the cell cycle and was used as a marker to identify cells in the S/G2 phase. Telomeres were detected by PNA-FISH. Fifty cells were analysed per condition in two independent experiments.

was inhibited (Figure 3B). TIF induction was accompanied by phosphorylation of Chk1 on Ser 345, the preferential target for phosphorylation by ATR kinase (29), in cells expressing ΔMTRF1 or ΔBΔM TRF2 (although less prominent) (Figure 3C). Conversely, ΔBΔMTRF2-expressing cells showed preferential phosphorylation of ATM and Chk2 (Figure 3C). This difference was not due to different levels of DNA damage activation at telomeres because TIFs formation was comparable in ΔMTRF1- and ΔBΔMTRF2-expressing cells (Figure 3B). Finally, to determine which fraction of cells formed γ-H2AX foci, we performed a detailed cell-cycle analysis and found that TIFs induction occurred mainly in cells in S/G2 phases at early time points after TRF1 and TRF2 knockdown with siRNAs (Figure 3D).

Telomere uncapping, rather than shortening, probably accounted for the observed phenotypes because telomere length did not seem to be altered in early passage ΔMTRF1 and ΔBΔMTRF2 cells (Supplementary Figure S3A). Therefore, TRF1 or TRF2 inhibition might switch telomeres to a senescence-signalling state by disrupting the shelterin complex. Although POT1, TIN2 and TRF2 expression in whole-cell lysates appeared unaltered by immunoblotting, they were severely depleted from the chromatin-bound fraction in ΔMTRF1 cells (Supplementary Figure S3B and S3C). In contrast, the amount of hRap1 recovered in the chromatin-bound fraction was unaltered (Supplementary Figure S3B). Immunofluorescence analysis confirmed that ΔMTRF1 expression led to loss of the punctuated telomeric signal of POT1, TIN2 and TRF2 (Supplementary Figure S4). These results suggest that TRF1 inhibition hinders TRF2 accumulation at chromosome ends and affects POT1 and TIN2 accumulation at telomeres, consistent with their dependence on TRF1 for telomere

binding (2). Although hRap1 expression in whole-cell lysates appeared unaltered by immunoblotting (Supplementary Figure S3D), expression of ΔBΔMTRF2 led to a significant loss of hRap1 from telomeres as shown by cell fractionation and immunofluorescence experiments, consistent with its dependence on TRF2 for telomere binding (Supplementary Figures S3B and S4). In contrast, the amount of TRF1, TIN2 and POT1 recovered in the chromatin-bound fraction was unaltered (Supplementary Figure S3B).

These results show that telomere proteins are required for efficient capping of telomeres in the G2 phase of the cell cycle. Higher occurrence of TIFs in G2 in pre-senescent fibroblasts may therefore reflect the fact that shorter telomeres are more prone to remain uncapped after replication.

Telomere capping is monitored in G2 by the ATM- and ATR-dependent damage responses

To test the role of ATM and/or ATR in monitoring telomere integrity, we monitored TIFs formation upon ATM and/or ATR inhibition in cells over-expressing ΔMTRF1 or ΔBΔMTRF2 and in which telomeres are deprotected. Treatment with the PI3K inhibitor caffeine completely blocked TIF induction in these cells, indicating that telomere damage signalling involves ATM and/or ATR kinases (Supplementary Figure S5A and S5B). In addition, the knock down of ATR or ATM by RNA interference experiments (Supplementary Figure S5C) showed that ATR was involved in H2AX phosphorylation following ΔMTRF1 over-expression, whereas both ATM and ATR (to a lesser extent) could play a role in the damage response following ΔBΔMTRF2 over-expression (Supplementary Figure S5A and S5B).

To further test the importance of the ATM and ATR pathways in the activation of the DNA damage response in G2, we monitored γ-H2AX and 53BP1 (another mediator of the DNA damage response) foci formation at telomeres, upon inhibition of ATM and ATR in pre-senescent cells. Inhibition of both ATM and ATR by caffeine decreased significantly γ-H2AX and 53BP1 foci formation at telomeres (Figure 4). The knockdown by siRNA of ATR and particularly of ATM markedly reduced the percentage of TIF-positive pre-senescent cells in G2 (Figure 4A and C). These data indicate that, in pre-senescent fibroblasts, telomere dysfunction in G2 triggers the full activation of both the ATM- and ATR-DNA damage response.

p53 and pRb block mitotic entry of cells with dysfunctional telomeres

Cells expressing ΔMTRF1 and ΔBΔMTRF2 ceased rapidly to proliferate and had a reduced rate of BrdU incorporation compared to control cells (Supplementary Figure S6A and S6B). This proliferative arrest was accompanied by biochemical changes that occur typically

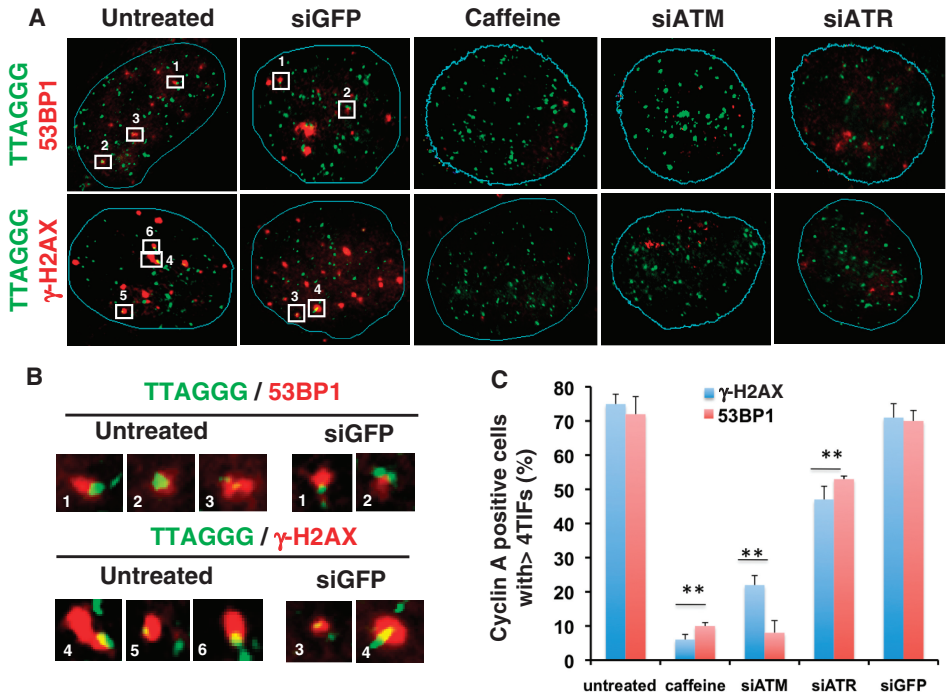

Figure 4. ATM- and ATR-dependency of TIFs formation in late S/G2 in pre-senescent fibroblasts. (**A**) Images of 53BP1 or γ-H2AX immunoFISH detection in Cyclin A-positive pre-senescent cells treated as indicated. Pre-senescent HFF cells (PD69) were treated with caffeine or transfected with si*ATM* or si*ATR* or si*GFP* and immunolabelled with anti-53BP1, anti-γ-H2AX, (red) and Cyclin A antibodies and processed by PNA-FISH to visualize telomeres (TTAGGG, green). (**B**) Enlarged colocalizing foci images, including the areas marked with white rectangles in (A). (**C**) Quantification of Cyclin A-positive cells exhibiting more than four γ-H2AX or 53BP1 telomeric foci (TIFs) in pre-senescent cells following incubation with caffeine or transfection with si*ATM*, si*ATR* or si*GFP*. Cells were prepared 48 h after transfection as in (A). The mean (±SD) of three independent experiments is reported. Statistical significance of the differences between untreated and treated cultures was assessed by Student's *t*-test (**$P < 0.001$).

during senescence: staining for SA-β Gal, decreased pRB phosphorylation, reduction of cyclin A and up-regulation of the cyclin-dependent kinase (Cdk) inhibitor p16 (Supplementary Figure S6C and S6D). Immunoblotting analysis to further characterize the DNA damage response in cells expressing ΔMTRF1 and ΔBΔMTRF2 revealed increased expression of total p53, of its Ser15 phosphorylated form [an event mediated by ATM/ATR kinases (29,30)] and of the Cdk inhibitor p21, a direct p53 transcriptional target (Supplementary Figure S6D).

To evaluate whether p53 and pRB play a role in preventing mitotic entry of cells with persistent uncapped telomeres in G2, early passage cells were infected with retroviruses expressing HPV16-E6/E7 (E6/E7 cells), two viral oncoproteins known to inhibit these tumour suppressors and then with retroviruses expressing ΔMTRF1 or ΔBΔMTRF2. E6 and E7 expression allowed bypassing the growth arrest and senescence phenotype due to ΔMTRF1 or ΔBΔMTRF2 expression (Supplementary Figure S6E). This facilitated the isolation of metaphase chromosomes, which could not be done in cells expressing only ΔMTRF1 or ΔBΔMTRF2 due to the low number of mitotic cells and the analysis of the fate of uncapped telomeres during mitosis by telomere PNA-FISH. ΔMTRF1 or ΔBΔMTRF2 over-expression in E6/E7 cells resulted in increased frequency (4- to 5-fold and 10- to 14-fold, respectively, $P < 0.0001$) of sister chromatid fusions compared to empty vector controls and E6/E7 cells over-expressing TRF1 and TRF2 (Figure 5A and B). On an average, metaphases isolated from control IMR-E6/E7 and HFF-E6/E7 cells displayed 0.04 and 0.10 events, respectively (Figure 5B). Moreover, in most cells with sister chromatid fusions, telomere DNA was detected (Figure 5A, panel b), indicating that such events occurred in the absence of total telomere deletion (31). E6/E7 cells over-expressing ΔMTRF1 or ΔBΔMTRF2 also showed a significant increase in chromosome ends with multi-telomeric signals [MTS, characterized by the presence of an extra-telomeric signal at one chromatid end (Figure 5A, panel c and C)], which is a direct indicator of telomere fragility resulting from replication fork stalling within the telomeric sequences (21,22). In addition, sister telomere losses [loss of telomere signal at only one chromatid end (Figure 5A, panel d) (32)] and telomere deletions [lack of telomere signals at both sister chromatids (Figure 5A, panel e)], but not end-to-end chromosome fusions (dicentric) (Figure 5A, panel f), were increased in E6/E7 cells expressing ΔMTRF1 (Figure 5D–F). Sister telomere loss and telomere deletion are thought to result from replication-associated telomere defects. Specifically, sister telomere loss might arise from S- or G2-specific post-replicative defects that affect only a single chromatid, whereas telomere deletion might be due to pre-replicative telomere dysfunction copied during S phase. Conversely, in E6/E7 cells expressing ΔBΔMTRF2 the frequencies of sister telomere losses and telomere deletions did not change appreciably relative to controls, whereas the frequency of dicentric chromosomes increased between 16- and 25-fold ($P < 0.0001$; Figure 5D–F). This suggests that dicentric chromosomes produced by TRF2 inhibition may instead reflect telomere uncapping (31). Therefore, our results suggest that in human primary fibroblasts, p53 and pRb block mitotic entry until all telomeres are properly processed in G2 to prevent telomere-dependent chromosomal abnormalities.

We have also observed an increase in sister chromatid-type telomere aberrations in pre-senescent HFF and IMR-90 cells whereas sister chromatid fusions and chromosome fusions were exceedingly rare or not present at all (Figure 6). Sister telomere losses were the most frequent telomere aberrations in pre-senescent cells and the percentage of chromosomes ends with multi-telomeric signals and terminal deletion increased in pre-senescent compared to younger cells (Figure 6B), indicating that defects of telomere post-replicative events increased with age. Therefore, telomere instability leading to DNA damage response in G2 in pre-senescent cells is distinct from telomere dysfunction that results in chromosome end-to-end fusions.

Extended G2 phase in pre-senescent fibroblasts is associated with p53 activation

Since DNA damage signalling in G2 in normal cells leads to cell cycle arrest, which is mainly triggered by the p53 pathway (24), we investigated p53 activation by monitoring the accumulation of the Cdk inhibitor p21, a p53 transcriptional target, in aging fibroblasts. p21 accumulation started very early, at PD73 many PDs before senescence (Figure 7A). Coincident with the increase in p21 levels, the ratio of hyperphosphorylated pRB to dephosphorylated pRB decreased very early at PD73 (Figure 7A), suggesting that p21 targets proteins regulated by the activity of Cdks. We first compared the expression of various cell cycle proteins between young proliferating, pre-senescent and fully senescent fibroblasts (no growth potential left). We found that the levels of Cyclin D1, A and E, Cdk2, Cdk4 and p16 were essentially unchanged at PD73 while the expression patterns of Cyclins and Cdk2 were altered in fully senescent cells (PD87). No significant changes in the levels of Cdk4 and Cdk6 were observed in HFF cells of any age (Figure 7A and data not shown). The changes in Cyclin D1, A and E levels, however, correlated with p16 accumulation whereas p21 expression peaked at PD82 (BrdU labelling index <10%) and declined thereafter in fully senescent cells, although its level remained higher than in young cells (Figure 7A).

As Cyclin A/Cdk activation can be blocked by ATM/ATR kinases signalling through p53-mediated up-regulation of p21, which directly inactivates Cyclin/Cdk complexes, we next analysed the Cyclin A-associated kinase activity, which controls S-phase progression and contributes to the G2/M transition entry (33–35), with an immunoprecipitation-kinase assay using Histone H1 as substrate. We found that the Cyclin A-associated kinase activity was markedly reduced in PD69 cells (Figure 7B) concomitantly with the increase in p21 levels (Figure 7A). Although Cyclin A remained associated with Cdk2 in pre-senescent cells, Cyclin A complexes contained increased levels of p21 as indicated by co-immunoprecipitation experiments, in comparison to young cells (Figure 7C). These changes are consistent with

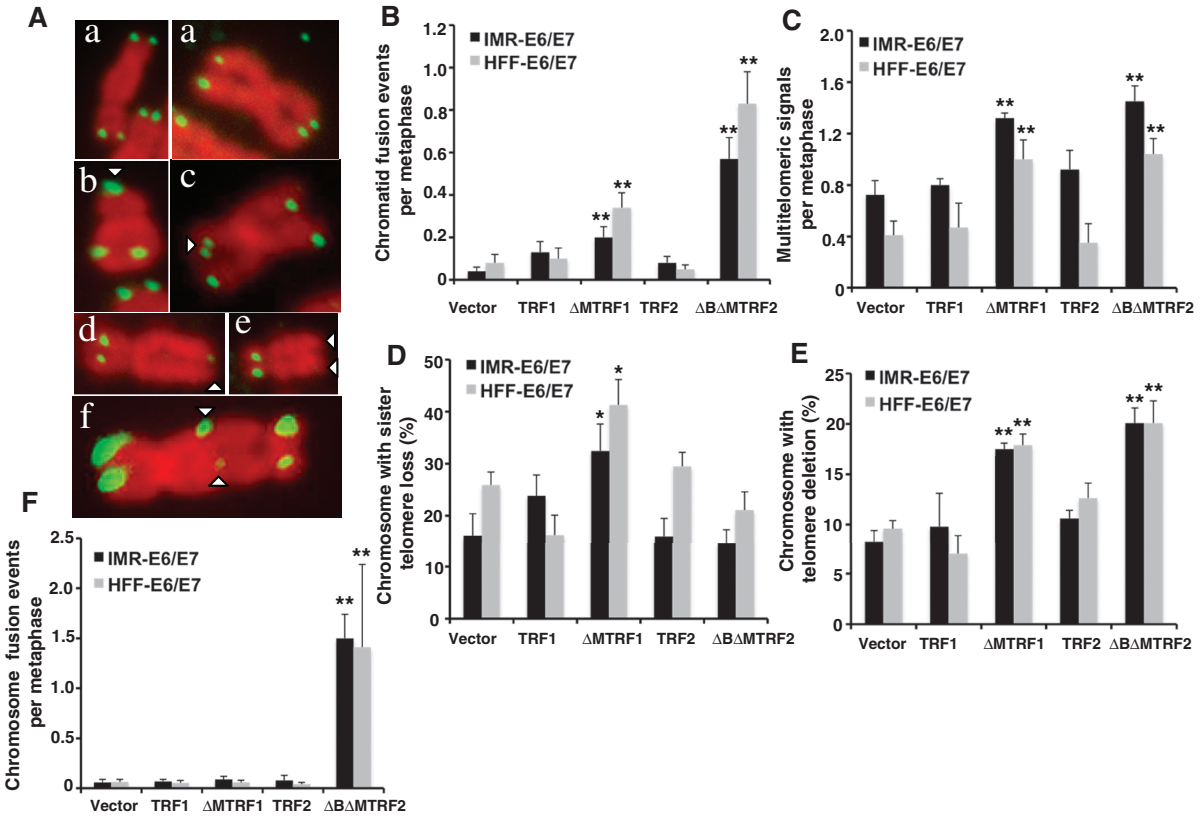

Figure 5. Chromosomal aberrations in fibroblasts expressing ΔMTRF1 or ΔBΔMTRF2. (**A**) Individual aberrations in E6/E7 cells expressing ΔMTRF1 or ΔBΔMTRF2. HFF cells expressing ΔMTRF1 (b–e), ΔBΔMTRF2 (f) or vector only (a) were collected and analysed by telomere PNA-FISH. Telomeres are shown in green and Hoechst-counterstained chromosomes in red (false colour). Arrowheads indicate chromosomal aberrations (b–f). Normal telomere (a), chromatid fusion (b), multi-telomeric signal (c), sister telomere loss (d), terminal deletion (e) and chromosome fusion (f). (**B–F**) Quantification of chromatid fusion (B), multi-telomeric signal (C), sister telomere loss (D), terminal deletion (E) and chromosomal end-to-end fusion (F) frequency in IMR-E6/E7 and HFF-E6/E7 cells expressing the indicated constructs. The mean (±SD) of three independent experiments is reported; at least 50 metaphases per cell type (**t-test P-value <0.001; **$P < 0.001$).

the prolonged S/G2 phase of pre-senescent compared to young cells (Figure 7D). Knockdown of p53 by shRNA in cells at PD69 resulted in significant increased Cyclin A-associated kinase activity and reduction of nuclear colocalization of p21 and Cyclin A (Figure 7B, C and E). Similar effect but to a lesser degree was obtained by shRNA-mediated knockdown of the ATM kinase (Figure 7B, C and E). These data confirm the involvement of the ATM kinase in sensing telomere damage and suggest that p21 acts downstream of p53 in response to telomere dysfunction in G2 in human fibroblasts.

DISCUSSION

Short telomeres or defects in telomere proteins can activate a checkpoint response that results in cell cycle arrest or apoptosis depending on the cellular background (6–8,36,37). An ATM- and p53-dependent checkpoint that detects altered telomere states at the G1/S transition was proposed to act as a regulator of the cellular response to telomere damage (37). Here we provide evidence that telomere shortening over successive cell divisions triggers a p53-dependent G2 checkpoint response that involves the ATM and ATR-dependent DNA damage signalling pathways. At each cell cycle, during a short time window, functional telomeres can be perceived and treated as double-strand breaks (DSB), thus rendering them temporarily dysfunctional, as evidenced by the transient recruitment of DNA damage sensors and repair proteins (3). These factors initiate the reactions required for telomere elongation, processing and capping (3) as well as reactions related to DNA repair by homologous recombination needed for the assembly of new functional telomeres (4). Telomere proteins should limit the duration of such telomere processing to a narrow interval just after conventional replication had been completed. We propose that, in the absence of telomerase, chronic telomere shortening and the concomitant imbalances of telomere proteins that occur in senescing cells affect proper telomere replication and end-protection. Short telomeres might thus be more prone to persist in an uncapped state and to trigger the p53-dependent G2 checkpoint response. In such cells, the ATM/ATR kinases, which are sensors of open telomere states, are activated and p53 acts as an effector to delay mitotic entry and halt the cell cycle in a state that favours the re-establishment of post-replicative telomere end-processing and protection.

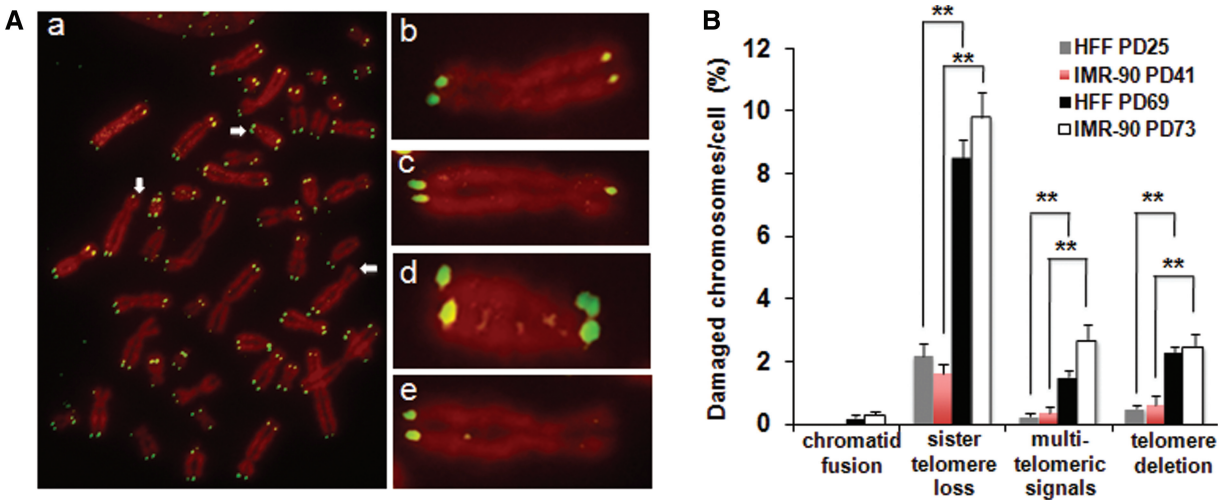

Figure 6. Telomere instability in pre-senescent fibroblasts. (**A**) Metaphase spread of pre-senescent HFF cells hybridized with a PNA telomere probe (green) (a). Examples of chromosomal aberrations are indicated by arrows in (a) and enlarged in (c–e). Normal telomere (b), sister telomere loss (c), multi-telomeric signal (d) and terminal deletion (e). (**B**) Quantification of the indicated chromosomal aberrations per cell in young and pre-senescent IMR-90 and HFF cells. The mean (±SD) of three independent experiments is reported; at least 30 metaphases per cell type (**t-test P-value <0.001).

Our results suggest that aging fibroblasts suffer from post-replicative telomere damage owing to telomere shortening. Unlike chromosome ends with adequate telomere length, in which DNA damage occurs transiently during the G2 phase of the cell cycle, in aging cells, damage would persist at a subset of the shortest telomeres, activating a full DNA damage response. The ability of TRF2 and possibly of other telomere proteins to participate in the telomere protective structure formation and stabilization (4,38,39) suggests that these proteins are required to ensure telomere integrity in the G2 phase after replication. Here, we show that telomere dysfunction through inhibition of TRF1 or TRF2 function leads to persistence of TIFs in G2, implying that down-regulation or functional imbalance of these proteins could account for telomere deprotection in G2 despite the presence of long telomeres. In addition, the threshold abundance of telomere proteins required to block chromosome fusions must be lower than the levels required for repressing the DNA damage response. This is supported by the observation that cells expressing ΔMTRF1, despite showing a DNA damage response at chromosomes ends, fail to exhibit massive chromosomal end-to-end fusions. This finding implies that in such cells, the chromosome ends maintain the capacity to suppress fusions through the retention of sufficient shelterin components, such as TRF2, to block the NHEJ pathway. Conversely, TRF2 inhibition in cells expressing ΔBΔMTRF2 led to fully uncapped telomeres, resulting in chromosome fusions. In such cells, the fusogenic state would arise because chromosome ends do not retain sufficient levels of shelterin to block the NHEJ pathway. Thus, in pre-senescent cells, the DNA damage response in G2 may result from insufficient levels of shelterin proteins; however, sufficient telomere protection is retained to prevent NHEJ as the frequency of chromosome fusions is rare in aging fibroblasts.

The observed telomere DNA damage response might also reflect abnormalities in stalled or collapsed replication forks, which can induce the ATR-H2AX/Chk1 signalling cascade, followed by DSB formation and consequent activation of the ATM-H2AX/Chk2-p53 pathway (29,30). Telomere proteins facilitate replication fork movement along the telomere and are critical to ensure faithful replication of telomeres (40). For example, TRF1 and TRF2 interact with and stimulate the RecQ-like helicases BLM and WRN (21,41,42), suggesting that they recruit these proteins to enable efficient replication and/or repair at the telomeres. It is not yet clear why short telomeres would be sensitive to replication fork progression, although one possibility is that chromatin changes at shortened telomeres (43) might contribute to increased replication stalling and thus stretch of single-stranded DNA formation. Upon ΔMTRF1 expression, chromosomes showed an increased frequency of chromatid aberrations, which might be due to defective telomere replication. Indeed, multi-telomeric signals result from incomplete replication or processing of stalled forks, leading to altered packaging and/or condensation of chromatin due to extended areas of single-stranded DNA, as suggested for fragile telomeres (21). This is in agreement with the hypothesis that alteration in the composition of the shelterin complex interferes with terminal processing.

Our data reveal that senescing cells spend an increasing amount of time in G2. Perhaps, a single defective (but not critically short) telomere is sufficient to activate a transient G2 checkpoint arrest signal and, as more telomeres become defective, this signal exceeds a damage threshold, resulting in a progressively prolonged G2 arrest. It is conceivable that the initial adaptation to this extended G2 phase allows cells to avoid NHEJ for completing the processing of telomere ends before proceeding with the cell division. In this case, the transient arrest would not be expected to block the growth of cells. However, the use of NHEJ to repair multiples post-replicative dysfunctional (critically uncapped short) telomere ends would lead to telomere fusions that allow cells to overcome the

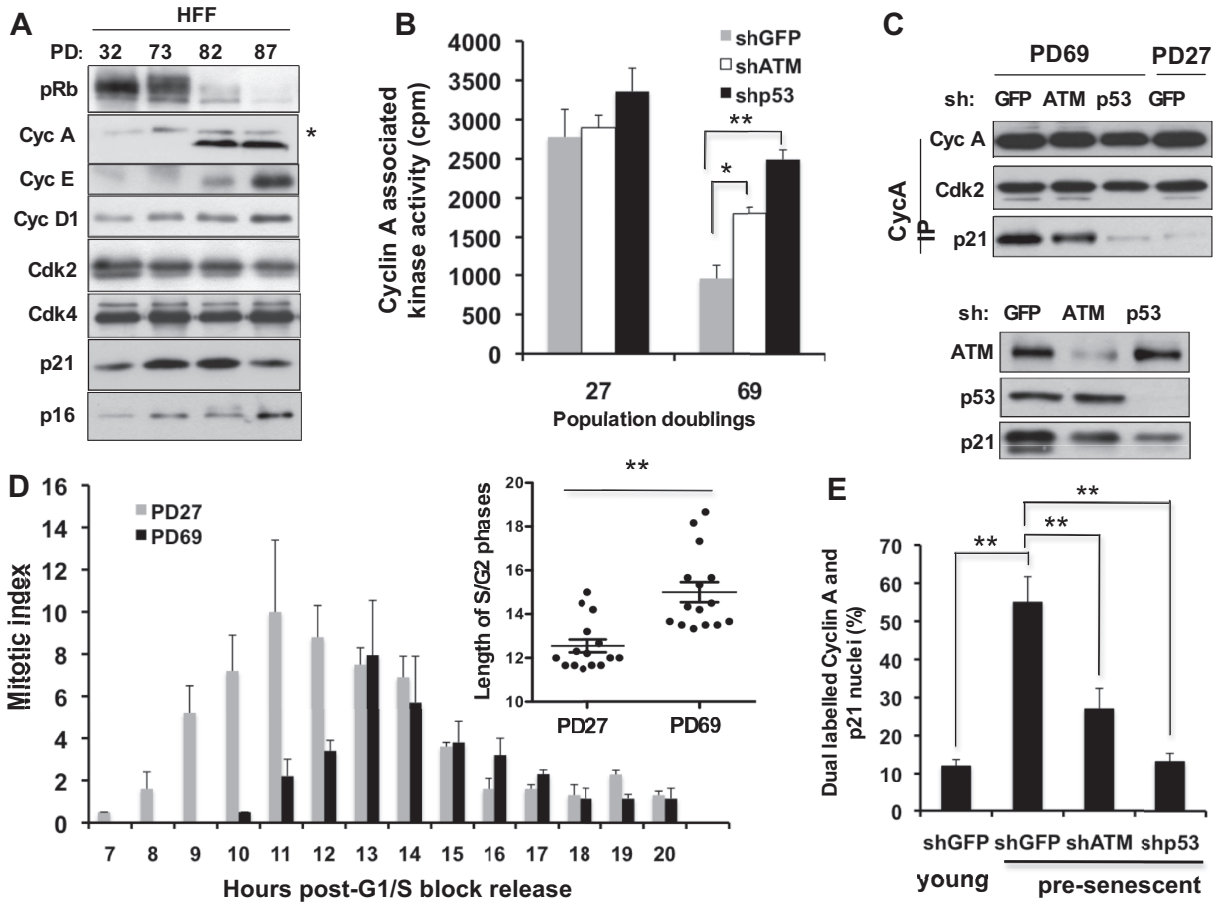

Figure 7. Consequences of the activation of the DNA damage checkpoint in late S/G2 in pre-senescent fibroblasts. (**A**) Expression levels of cell cycle regulators during replicative aging. Western-blot analysis of HFF cells cultured until senescence and probed for the indicated proteins. Asterisk indicates a non-specific band. (**B**) Impaired Cyclin A-associated kinase activity in pre-senescent cells is dependent on p53 expression. The histogram shows Cyclin A-associated kinase activity of Cyclin A immunoprecipitates from HFF cells at PD69 infected with shATM, shp53 or shGFP (control) constructs and assayed *in vitro* using Histone H1 as substrate. The mean (±SD) of three independent experiments is reported (*t-test P-value <0.01; **$P < 0.001$). (**C**) Cyclin A immunoprecipitates (CycA IP) from pre-senescent cells at PD69 and young cells at PD27 expressing the indicated shRNAs were analysed by immunoblotting for Cdk2 and p21 interaction (upper panel). Immunoblots showing ATM, p53 and p21 expression in HFF cells at PD69 infected with the indicated shRNAs (lower panel). (**D**) Average lengthening of the S/G2 phase in pre-senescent (PD69) when compared to young (PD27) fibroblasts. Cells were synchronized at the G1/S transition by hydroxyurea block and released into fresh media. Entry into mitosis was gauged by scoring phospho-H3 positive cells following immunofluorescence of fixed cells at the indicated time points after release. The insert shows the distribution of the length (hours) of the S/G2 phase in 15 analyses for each culture (**t-test P-value <0.001). (**E**) Quantification of co-expression of Cyclin A and p21 in nuclei of young and pre-senescent HFF cells expressing the indicated shRNAs. Cells were analysed 8 days post-infection by double-immunofluorescence for Cyclin A and p21 expression. The mean (±SD) of three independent experiments is shown (*t-test P-value <0.01; **$P < 0.001$).

checkpoint arrest and eventually to progress to G1, where the permanent cell cycle arrest and senescence program will be engaged in response to breaks induced by chromosome fusions following mitosis. Alternatively, the persistence of physiologically uncapped telomeres in G2 may send a qualitatively different signal that results in arrest during the next cell cycle. Our findings challenge the current paradigm that the checkpoint response to eroded telomeres occurs primarily at the G1/S transition in human cells.

SUPPLEMENTARY DATA

Supplementary Data are available at NAR Online: Supplementary Figures 1–6.

ACKNOWLEDGEMENTS

We thank Montpellier RIO Imaging facility for expert assistance, Dr P. Fort for help with statistical analyses and Drs T. De Lange, D. Galloway, F. d'Adda di Fagagna and S.-H. Kim for sharing cells, plasmids and antibodies. L.J. and V.G. designed the research; L.J., M.M. and V.G. performed the research; L.J. and V.G. analysed the data; V.G. wrote the paper and P.R. financed the project.

FUNDING

Fondation de France grant (to V.G. and P.R.); Ligue contre le Cancer de L'Hérault (doctoral fellowship to L.J. and grant to V.G.); Association pour la Recherche

contre le Cancer (ARC) (to L.J. and grant ARC 4028 to P.R.) and Société Française du Cancer (to L.J.). Funding for open access charge: ARC 4028.

Conflict of interest statement. None declared.

REFERENCES

1. Blackburn,E.H. (2001) Switching and signaling at the telomere. *Cell*, **106**, 661–673.
2. de Lange,T. (2005) Shelterin: the protein complex that shapes and safeguards human telomeres. *Genes Dev.*, **19**, 2100–2110.
3. Verdun,R.E., Crabbe,L., Haggblom,C. and Karlseder,J. (2005) Functional human telomeres are recognized as DNA damage in G2 of the cell cycle. *Mol. Cell*, **20**, 551–561.
4. Verdun,R.E. and Karlseder,J. (2006) The DNA damage machinery and homologous recombination pathway act consecutively to protect human telomeres. *Cell*, **127**, 709–720.
5. Harley,C.B., Futcher,A.B. and Greider,C.W. (1990) Telomeres shorten during ageing of human fibroblasts. *Nature*, **345**, 458–460.
6. d'Adda di Fagagna,F., Reaper,P.M., Clay-Farrace,L., Fiegler,H., Carr,P., Von Zglinicki,T., Saretzki,G., Carter,N.P. and Jackson,S.P. (2003) A DNA damage checkpoint response in telomere-initiated senescence. *Nature*, **426**, 194–198.
7. Herbig,U., Jobling,W.A., Chen,B.P., Chen,D.J. and Sedivy,J.M. (2004) Telomere shortening triggers senescence of human cells through a pathway involving ATM, p53, and p21(CIP1), but not p16(INK4a). *Mol. Cell*, **14**, 501–513.
8. Gire,V., Roux,P., Wynford-Thomas,D., Brondello,J.M. and Dulic,V. (2004) DNA damage checkpoint kinase Chk2 triggers replicative senescence. *EMBO J.*, **23**, 2554–2563.
9. Bodnar,A.G., Ouellette,M., Frolkis,M., Holt,S.E., Chiu,C.P., Morin,G.B., Harley,C.B., Shay,J.W., Lichtsteiner,S. and Wright,W.E. (1998) Extension of life-span by introduction of telomerase into normal human cells. *Science*, **279**, 349–352.
10. Baird,D.M., Rowson,J., Wynford-Thomas,D. and Kipling,D. (2003) Extensive allelic variation and ultrashort telomeres in senescent human cells. *Nat. Genet.*, **33**, 203–207.
11. Zhu,J., Wang,H., Bishop,J.M. and Blackburn,E.H. (1999) Telomerase extends the lifespan of virus-transformed human cells without net telomere lengthening. *Proc. Natl Acad. Sci. USA*, **96**, 3723–3728.
12. Ouellette,M.M., Liao,M., Herbert,B.S., Johnson,M., Holt,S.E., Liss,H.S., Shay,J.W. and Wright,W.E. (2000) Subsenescent telomere lengths in fibroblasts immortalized by limiting amounts of telomerase. *J. Biol. Chem.*, **275**, 10072–10076.
13. Karlseder,J., Smogorzewska,A. and de Lange,T. (2002) Senescence induced by altered telomere state, not telomere loss. *Science*, **295**, 2446–2449.
14. de Lange,T. (2002) Protection of mammalian telomeres. *Oncogene*, **21**, 532–540.
15. Hemann,M.T., Strong,M.A., Hao,L.Y. and Greider,C.W. (2001) The shortest telomere, not average telomere length, is critical for cell viability and chromosome stability. *Cell*, **107**, 67–77.
16. Abdallah,P., Luciano,P., Runge,K.W., Lisby,M., Geli,V., Gilson,E. and Teixeira,M.T. (2009) A two-step model for senescence triggered by a single critically short telomere. *Nat. Cell Biol.*, **11**, 988–993.
17. Zhu,X.D., Niedernhofer,L., Kuster,B., Mann,M., Hoeijmakers,J.H. and de Lange,T. (2003) ERCC1/XPF removes the 3' overhang from uncapped telomeres and represses formation of telomeric DNA-containing double minute chromosomes. *Mol. Cell*, **12**, 1489–1498.
18. van Steensel,B., Smogorzewska,A. and de Lange,T. (1998) TRF2 protects human telomeres from end-to-end fusions. *Cell*, **92**, 401–413.
19. Celli,G.B. and de Lange,T. (2005) DNA processing is not required for ATM-mediated telomere damage response after TRF2 deletion. *Nat. Cell Biol.*, **7**, 712–718.
20. Smogorzewska,A. and de Lange,T. (2002) Different telomere damage signaling pathways in human and mouse cells. *EMBO J.*, **21**, 4338–4348.
21. Sfeir,A., Kosiyatrakul,S.T., Hockemeyer,D., MacRae,S.L., Karlseder,J., Schildkraut,C.L. and de Lange,T. (2009) Mammalian telomeres resemble fragile sites and require TRF1 for efficient replication. *Cell*, **138**, 90–103.
22. Martinez,P., Thanasoula,M., Munoz,P., Liao,C., Tejera,A., McNees,C., Flores,J.M., Fernandez-Capetillo,O., Tarsounas,M. and Blasco,M.A. (2009) Increased telomere fragility and fusions resulting from TRF1 deficiency lead to degenerative pathologies and increased cancer in mice. *Genes Dev.*, **23**, 2060–2075.
23. Thanasoula,M., Escandell,J.M., Martinez,P., Badie,S., Munoz,P., Blasco,M.A. and Tarsounas,M. (2010) p53 prevents entry into mitosis with uncapped telomeres. *Curr. Biol.*, **20**, 521–526.
24. Baus,F., Gire,V., Fisher,D., Piette,J. and Dulic,V. (2003) Permanent cell cycle exit in G2 phase after DNA damage in normal human fibroblasts. *EMBO J.*, **22**, 3992–4002.
25. van Steensel,B. and de Lange,T. (1997) Control of telomere length by the human telomeric protein TRF1. *Nature*, **385**, 740–743.
26. Cawthon,R.M. (2002) Telomere measurement by quantitative PCR. *Nucleic Acids Res.*, **30**, e47.
27. Gire,V. (2004) Dysfunctional telomeres at senescence signal cell cycle arrest via Chk2. *Cell Cycle*, 3.
28. Takai,H., Smogorzewska,A. and de Lange,T. (2003) DNA damage foci at dysfunctional telomeres. *Curr. Biol.*, **13**, 1549–1556.
29. Shiloh,Y. (2003) ATM and related protein kinases: safeguarding genome integrity. *Nat. Rev. Cancer*, **3**, 155–168.
30. Kastan,M.B. and Bartek,J. (2004) Cell-cycle checkpoints and cancer. *Nature*, **432**, 316–323.
31. Smogorzewska,A., Karlseder,J., Holtgreve-Grez,H., Jauch,A. and de Lange,T. (2002) DNA ligase IV-dependent NHEJ of deprotected mammalian telomeres in G1 and G2. *Curr. Biol.*, **12**, 1635–1644.
32. Crabbe,L., Verdun,R.E., Haggblom,C.I. and Karlseder,J. (2004) Defective telomere lagging strand synthesis in cells lacking WRN helicase activity. *Science*, **306**, 1951–1953.
33. Yam,C.H., Fung,T.K. and Poon,R.Y. (2002) Cyclin A in cell cycle control and cancer. *Cell. Mol. Life Sci.*, **59**, 1317–1326.
34. Furuno,N., den Elzen,N. and Pines,J. (1999) Human cyclin A is required for mitosis until mid prophase. *J. Cell Biol.*, **147**, 295–306.
35. Pagano,M., Pepperkok,R., Verde,F., Ansorge,W. and Draetta,G. (1992) Cyclin A is required at two points in the human cell cycle. *EMBO J.*, **11**, 961–971.
36. Lee,H.W., Blasco,M.A., Gottlieb,G.J., Horner,J.W. 2nd, Greider,C.W. and DePinho,R.A. (1998) Essential role of mouse telomerase in highly proliferative organs. *Nature*, **392**, 569–574.
37. Karlseder,J., Broccoli,D., Dai,Y., Hardy,S. and de Lange,T. (1999) p53- and ATM-dependent apoptosis induced by telomeres lacking TRF2. *Science*, **283**, 1321–1325.
38. Stansel,R.M., de Lange,T. and Griffith,J.D. (2001) T-loop assembly in vitro involves binding of TRF2 near the 3′ telomeric overhang. *EMBO J.*, **20**, 5532–5540.
39. Bianchi,A., Stansel,R.M., Fairall,L., Griffith,J.D., Rhodes,D. and de Lange,T. (1999) TRF1 binds a bipartite telomeric site with extreme spatial flexibility. *EMBO J.*, **18**, 5735–5744.
40. Gilson,E. and Geli,V. (2007) How telomeres are replicated. *Nat. Rev. Mol. Cell Biol.*, **8**, 825–838.
41. Lillard-Wetherell,K., Machwe,A., Langland,G.T., Combs,K.A., Behbehani,G.K., Schonberg,S.A., German,J., Turchi,J.J., Orren,D.K. and Groden,J. (2004) Association and regulation of the BLM helicase by the telomere proteins TRF1 and TRF2. *Hum. Mol. Genet.*, **13**, 1919–1932.
42. Opresko,P.L., Otterlei,M., Graakjaer,J., Bruheim,P., Dawut,L., Kolvraa,S., May,A., Seidman,M.M. and Bohr,V.A. (2004) The Werner syndrome helicase and exonuclease cooperate to resolve telomeric D loops in a manner regulated by TRF1 and TRF2. *Mol. Cell*, **14**, 763–774.
43. O'Sullivan,R.J., Kubicek,S., Schreiber,S.L. and Karlseder,J. (2010) Reduced histone biosynthesis and chromatin changes arising from a damage signal at telomeres. *Nat. Struct. Mol. Biol.*, **17**, 1218–1225.